AIP | Review of Scientific Instruments

Development of imaging bolometers for magnetic fusion reactors (invited)

Byron J. Peterson, Homaira Parchamy, Naoko Ashikawa, Hisato Kawashima, Shigeru Konoshima et al.

Citation: Rev. Sci. Instrum. **79**, 10E301 (2008); doi: 10.1063/1.2988822
View online: http://dx.doi.org/10.1063/1.2988822
View Table of Contents: http://rsi.aip.org/resource/1/RSINAK/v79/i10
Published by the American Institute of Physics.

Related Articles

Hydrogen transport diagnostics by atomic and molecular emission line profiles simultaneously measured for large helical device
Phys. Plasmas 20, 012514 (2013)

Time-and-space resolved comparison of plasma expansion velocities in high-power diodes with velvet cathodes
J. Appl. Phys. 113, 043307 (2013)

Development of a diffuse air-argon plasma source using a dielectric-barrier discharge at atmospheric pressure
Appl. Phys. Lett. 102, 033503 (2013)

Nonmonotonic radial distribution of excited atoms in a positive column of pulsed direct currect discharges in helium
Appl. Phys. Lett. 102, 034104 (2013)

Iterative Boltzmann plot method for temperature and pressure determination in a xenon high pressure discharge lamp
J. Appl. Phys. 113, 043303 (2013)

Additional information on Rev. Sci. Instrum.

Journal Homepage: http://rsi.aip.org
Journal Information: http://rsi.aip.org/about/about_the_journal
Top downloads: http://rsi.aip.org/features/most_downloaded
Information for Authors: http://rsi.aip.org/authors

ADVERTISEMENT

Development of imaging bolometers for magnetic fusion reactors (invited)[a)]

Byron J. Peterson,[1] Homaira Parchamy,[1] Naoko Ashikawa,[1] Hisato Kawashima,[2] Shigeru Konoshima,[2] Artem Yu. Kostryukov,[3] Igor V. Miroshnikov,[3] Dongcheol Seo,[4] and T. Omori[5]

[1]*National Institute for Fusion Science, Toki 509-5292, Japan*
[2]*Japan Atomic Energy Agency, Naka 311-0193, Japan*
[3]*St. Petersburg State Technical University, St. Petersburg 195251, Russia*
[4]*National Fusion Research Institute, Daejeon 305-333, Republic of Korea*
[5]*Graduate University for Advanced Studies, Toki 509-5292 Japan*

(Presented 12 May 2008; received 9 May 2008; accepted 25 August 2008; published online 31 October 2008)

Imaging bolometers utilize an infrared (IR) video camera to measure the change in temperature of a thin foil exposed to the plasma radiation, thereby avoiding the risks of conventional resistive bolometers related to electric cabling and vacuum feedthroughs in a reactor environment. A prototype of the IR imaging video bolometer (IRVB) has been installed and operated on the JT-60U tokamak demonstrating its applicability to a reactor environment and its ability to provide two-dimensional measurements of the radiation emissivity in a poloidal cross section. In this paper we review this development and present the first results of an upgraded version of this IRVB on JT-60U. This upgrade utilizes a state-of-the-art IR camera (FLIR/Indigo Phoenix-InSb) (3–5 μm, 256×360 pixels, 345 Hz, 11 mK) mounted in a neutron/gamma/magnetic shield behind a 3.6 m IR periscope consisting of CaF_2 optics and an aluminum mirror. The IRVB foil is 7 cm$\times$9 cm $\times$5 μm tantalum. A noise equivalent power density of 300 $\mu W/cm^2$ is achieved with 40×24 channels and a time response of 10 ms or 23 $\mu W/cm^2$ for 16×12 channels and a time response of 33 ms, which is 30 times better than the previous version of the IRVB on JT-60U. © *2008 American Institute of Physics.* [DOI: 10.1063/1.2988822]

I. INTRODUCTION

Resistive bolometers are commonly used in fusion experiments to measure the total radiated power. Ultimately they should provide a temporally and spatially resolved measurement of the radiation profile throughout the plasma cross section.[1] These detectors are based on the principle of the temperature dependence of the electrical resistance of a meander of metal. A thin foil (typically 4 μm of gold) is used to absorb the radiation whose energy is then transferred thermally through a Kapton, mica, or SiN insulating layer to the gold resistive meander. These detectors are highly developed utilizing a Wheatstone bridge consisting of four resistive legs, two of which measure the incoming radiation and two of which are shielded from the incoming radiation and form a background temperature reference.[2] This bridge circuit is intended to compensate the heating of the surrounding supporting structure using the reference resistors, however, if the characteristics of the reference and measuring resistors are not perfectly matched then a drift in signal with time can result. This drift not only produces a false signal but also with time can increase the signal level beyond the range of the analog to digital convertors. If the drift could be characterized (which may not be possible) the former effect could be subtracted off in the analysis, but the latter problem can only be solved by periodically shuttering the detectors and readjusting the balance of the bridge (resetting the signal to zero) or by lowering the amplifier gain, thereby reducing the sensitivity. The shuttering of resistive bolometers installed at various poloidal locations in the first wall may not be practical; therefore this signal drift may present a problem for the steady-state measurement of the total radiated power using resistive bolometers. Countermeasures involving the use of feedback control of additional resistive heating grids behind each of the four resistors are under development, but this would complicate the electronic circuitry and double the already large number of wires (four) necessary per channel.[3] A more likely solution to this problem is the use of laser trimming to match the resistances of the four legs.[4] This problem may be compounded by differences between the reference and sensing resistors in the absorption of nuclear heating. One solution to this problem would be to test the drift of each detector and reject those with unacceptably high values, but this would raise the cost per channel. Another problem experienced by resistive bolometers with a gold meander and absorber on a mica substrate in tests under reactor equivalent neutron fluxes is the loss of electrical contacts during the thermal variations incurred at the termination of the neutron exposure.[5] Alternative detector materials such as Pt on AlN and alumina have been satisfactorily tested in a nuclear environment[6] and platinum bonding techniques have been developed which are superior to the previous spring loaded contacts.[4] A prototype resistive bolometer with a 1.5 μm Pt

[a)]Invited paper, published as part of the Proceedings of the 17th Topical Conference on High-Temperature Plasma Diagnostics, Albuquerque, New Mexico, May 2008.

absorber on an SiN substrate has been produced and used successfully on ASDEX-Upgrade.[7] A prototype with a 3.5 μm Pt absorber and platinum bonded contacts has also been produced and tested in ASDEX-Upgrade and further radiation testing is planned.[4] Another unresolved issue for resistive bolometers is the thickness of the absorber foil. For ITER a thickness of 12 μm or more is expected while the thickest absorber fabricated to date is 8 μm of gold on a 20 μm mica substrate.[8] Additionally, due to the Wheatstone bridge circuit, a large number of wires (five per channel) are necessary for the resistive bolometers. This not only poses a risk in terms of vacuum reliability but also leaves the diagnostic susceptible to radiation induced electromotive force and other sources of noise.

As an alternative or complimentary diagnostic to resistive bolometers, imaging bolometers have been proposed. Imaging bolometers are similar to resistive bolometer in that they use a thin metal foil to absorb the photon and neutral flux from the plasma, but they differ in that the foil temperature is measured by an infrared (IR) camera instead of a resistive grid.[9] By transferring the foil temperature information from the vacuum vessel using IR radiation the problems of many wires in the case of the resistive bolometers are avoided. The IR imaging video bolometer (IRVB) uses a large thin foil to provide a time resolved image of the plasma radiation.[10,11] By solving the equation for the heat diffusion in the foil the two-dimensional distribution of the incident photon and neutral power is derived as a function of time. Since the foil temperatures are taken with respect to neighboring pixels or that of the surrounding and supporting thick (2×2 mm^2) copper frame (which temperature is also constantly measured by the IR camera), any temperature drift of the frame is automatically compensated for in the analysis. In addition, increasing the foil thickness is easy to do and should enhance the stiffness and uniformity of the foil. Therefore due to the radiation resistance of the materials used (copper frame and Pt, Ta or W foil), the lack of wires and the lack of signal drift, imaging bolometers represent an alternative to resistive bolometers for diagnosing radiation from a steady-state fusion reactor.

In this paper we describe the imaging bolometer by comparing two recent examples that have been installed and operated on the JT-60U device. In Sec. II the IRVB concept is described including data analysis and calibration techniques. In Sec. III the first IRVB installation in JT-60U and the current upgrade are compared. In Sec. IV a summary is given with further comparison with resistive bolometers and prospects for the applicability to ITER.

II. IMAGING BOLOMETER CONCEPT

A. Concept, data analysis, and calibration

The first realization of an imaging bolometer used segmented copper masks to sandwich the foil. The holes in the masks expose the foil on both sides forming the bolometer pixels.[9] Cooling of the foil by the masks and problems with cross-talk between the pixels because of poor thermal contact between the mask and foil led to the development of the IRVB which is the subject of this paper.[10,11] The IRVB exposes the entire foil except for the edge which is sandwiched by two frame pieces to support the foil. Instead of relying on the segmented mask to thermally isolate and define the bolometer pixels, the two-dimensional heat diffusion equation of the foil [given by Eq. (1)]

$$-\Omega_{\mathrm{rad}}+\Omega_{bb}+\frac{1}{\kappa}\frac{\partial T}{\partial t}=\frac{\partial^2 T}{\partial x^2}+\frac{\partial^2 T}{\partial y^2},$$

$$\Omega_{\mathrm{rad}}=\frac{P_{\mathrm{rad}}}{kt_f l^2}\quad \Omega_{bb}=\frac{\varepsilon\sigma_{\mathrm{SB}}(T^4-T_0^4)}{kt_f}, \tag{1}$$

is solved for the incident radiation, P_{rad}, by using the Crank–Nicholson algorithm from the two-dimensional temperature, T, distribution on the foil measured by an IR camera[11] where k is the foils thermal conductivity, t_f is the thickness of the foil, l is the dimension of the bolometer pixel, σ_{SB} is the Stefan–Boltzmann constant, ε is the blackbody emissivity, T_0 is the background temperature, and κ is the thermal diffusivity of the foil. In order to do so the IR camera must be calibrated for the foil temperature measurement and the local foil properties: κ, ε, and the product kt_f, must be determined through the foil calibration technique.[11,12]

B. Sensitivity

The sensitivity of the IRVB is given by the equation for noise equivalent power density (NEPD), S_{IRVB},[11,13]

$$S_{\mathrm{IRVB}}=\frac{\sqrt{2}kt_f\sigma_{\mathrm{IR}}}{\sqrt{f_{\mathrm{IR}}N_{\mathrm{IR}}}}\sqrt{\frac{5N_{\mathrm{bol}}^3 f_{\mathrm{bol}}}{A_f^2}+\frac{N_{\mathrm{bol}}f_{\mathrm{bol}}^3}{\kappa^2}}, \tag{2}$$

where σ_{IR} is the noise equivalent temperature of the IR camera, f_{IR} is the frame rate of the IR camera, A_f is the area of the bolometer foil, N_{IR} is the number of pixels of the IR camera which are used in the analysis, N_{bol} is the number of bolometer pixels, and f_{bol} is the frequency response of the IRVB. In Eq. (2) the blackbody radiation term is left out since it is negligible for foil temperatures which are less than 1000 °C. Usually the right hand term inside the radical dominates (for $N_{\mathrm{bol}}<1000$ and $f_{\mathrm{bol}}>100$ Hz) which can give an expression for the sensitivity (inversely proportional to NEPD) of the IRVB in terms of the foil parameters as κ/kt_f.

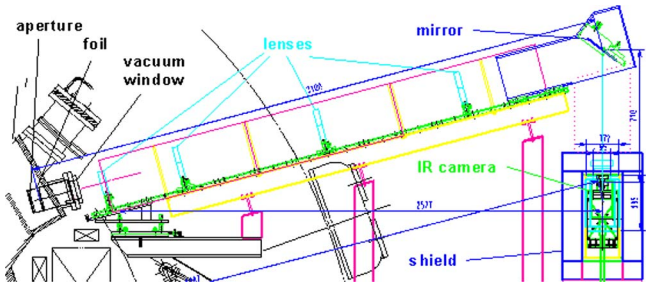

FIG. 1. (Color online) Schematic of optical system for the IRVB upgrade on JT-60U (Ref. 14) (© [2007] IEEE).

III. IRVB UPGRADE FOR JT-60U

This section describes the upgraded IRVB (Ref. 14) on JT-60U (shown in Fig. 1) and compares it with the previous version.[15]

A. Foil material

The choice of foil material is dictated by various characteristics of the foil including the ratio of thermal diffusivity to thermal conductivity (κ/k), which is a measure of the sensitivity of the IRVB, tensile strength, neutron cross section, melting point, ability to stop high energy photons, etc. In addition, practical considerations such as melting point and the availability of thin large foils should be evaluated. Such parameters have been considered[13] and the prime candidates for an IRVB foil are W, Ta, and Pt, whose properties are shown along with those of gold in Table I. While gold has been used previously, it is not suitable for use in a neutron rich reactor environment due to the tendency for transmutation to Hg (Ref. 5) and is only shown for comparison. Pt has the lowest neutron cross section, σ_{neutron}, and can stop the highest energy photons, but has the lowest sensitivity and tensile strength of the three. W may be the best choice for a reactor because of its superior strength and ability to stop relatively high energy photons; however, large foils of less than 10 μm thickness are not available. Since a thinner foil is needed for the JT-60U IRVB upgrade, we have chosen Ta to see the effects of a stronger foil material on the foil stability.

Calibration of the 5 μm Ta foil showed that the kt_f factor varies from 2.28 at the center to 2.24 at the edge relative to the nominal values, indicating good uniformity, but a large variation from the nominal values, leading to lower sensitivity. A 2.5 mm Au foil similar to that used previously in JT-60U showed a variation in the kt_f factor (relative to the nominal values) of 1.2–0.72 from the center to the edge indicating worse uniformity but values closer to the nominal value than those of the Ta foil. The reason for these variations from the nominal value is not clear.[16]

B. Foil thickness

A trade-off exists in the selection of the foil thickness between the sensitivity of the IRVB, which is inversely proportional to foil thickness, and the ability of the foil to stop high energy photons, which increases with foil thickness. The previously used gold foil with a nominal thickness of 2.5 μm could stop photons with energies up to ~8 keV. This is a little low for the high temperature plasmas in JT-60U, therefore we decided to use a thickness of the Ta foil of 5 μm. This will stop photons having energies of less than 9 keV and between 10 and 15 keV. This additional thickness will also stiffen the foil. The exposed size of the foil is 9 $\times 7$ cm^2 as in the previous case.

C. Infrared periscope

The IR periscope was designed to bring the IR signal to the IR camera located 2.4 m further away from the machine than the previous case to reduce the neutron flux and magnetic field and thus improve the shielding. The IR periscope consists of an IR vacuum window, four lenses, and a mirror. The entire setup is shown in Fig. 1. The total length of the optical path from the foil to the front surface of the IR camera body is 3.8 m. The resulting optical system is estimated to have an optical throughput of 0.025 which is 42 times better than of the previous case giving a 2.5 times improvement in the bolometer sensitivity. Previously a 58 mm diameter ZnSe window was used. This is replaced with a 100 mm diameter, 4 mm thick sapphire window. While the wavelength range of sapphire is not quite optimal for the 3–5 μm InSb detector in the IR camera, previous experience on JT-60U with sapphire windows provides some assurance that it can be used reliably. Measurements of the IR transmission of a similar window for a target at 150 °C give a value of 0.911. Four CaF_2 lenses are used to bring the image of the foil to the IR camera. The first (closest to window) lens has a diameter of 100 mm and the others have diameters of 150 mm. The IR camera uses a 100 mm focal length, $F/2.3$ lens with a $\frac{1}{4}$ in. extension. CaF_2 was chosen because it has one of the highest transmission levels for the 3–5 μm range of the InSb detector. There is some question about fluorescence, and darkening of CaF_2 during neutron and gamma radiations, but this has only been observed for certain wavelengths in the visible range. We hope to check for any degradation in IR transmission through recalibration of the optical system after the shutdown of JT-60U. The mirror is 20 cm diameter Al on

TABLE I. Properties of IRVB foil candidate materials (Ref. 14) (© [2007] IEEE).

	Tensile strength (MPa)	σ_{neutron} (barn)	K (W/m K) at 0–100 °C	κ/k (cm^3 K/J)	E_{ph} (keV) at 10 μm
Ta	760	22	57.5	0.43	20.1
Au	220	98.8	318	0.40	23.2
W	1920	18.5	173	0.39	21.4
Pt	200–300	9.0	71.6	0.35	23.9

a K8 glass base located between the last CaF_2 lens and the IR camera lens. The IR transmission measured with the Phoenix camera, $\frac{1}{4}$ in. extension, 100 mm lens and optical system was 0.996 compared to the same 150 °C object and field of view with only the Phoenix camera, extension and 100 mm lens. Including the transmission through the sapphire window the transmission is 0.908. The blackbody source used for the camera calibration and transmission measurements is a MIKRON M345Xx6.[17]

D. IR camera

The IR camera is a Phoenix Midwave (3–5 μm) by Indigo/FLIR with an InSb detector cooled by a Stirling cooler. The pixel number is 320×256 and the manufacturers rated sensitivity is <25 mK at room temperature. We achieved 11.2 mK sensitivity in operation at 150 °C on JT-60U which is about ten times the bit noise of 1.2 mK. For high gain operation this bit noise can be lowered to 0.4 mK. The data acquisition is 14 bit digital video data and the maximum frame rate for full frame is 345 Hz. This camera represents a significant improvement over the previously used Omega IR camera which used a microbolometer detector (7.5–13.5 μm) with a frame rate of 30 Hz, 160×128 pixels, and a nominal sensitivity of 100 mK. The bit noise level was 67 mK and typical experimental values of noise were two times higher. The resulting improvement in the IRVB sensitivity with the Phoenix IR camera compared to the Omega IR camera is on the order of 100. Sample data from the IR camera are shown in Fig. 2 after subtracting a reference image (taken prior to the discharge) to compensate for reflections by the foil of the surrounding structure between the IR camera and the foil. As long as the reflection does not change this reference image is valid. This requires that the temperature of the surrounding structure remain constant and that the foil does not move relative to the IR camera. Also the reflection is small due to the blackening of the foil and can be reduced by cooling the surrounding structure.

E. Shield

The shield consists of magnetic, gamma, and neutron shields. A 20 mm thick soft iron box was designed to shield the IR camera from stray magnetic fields up to 300 G which is above the expected maximum magnetic field at the IR camera location. Operation on JT-60U has shown the magnetic shield to be sufficient. We have not noticed any problems related to the ramp up or ramp down of the magnetic field with the new IRVB.

The neutron shield consists of a 10 cm thick shield made of a boron-doped material called eponite.[18] This shield against neutrons is surrounding a 20 mm thick lead shield against the secondary gamma rays produced in the eponite by the neutrons. The lead shield encompasses the soft iron shield (and IR camera), which should also provide some shielding of the secondary gamma rays. In the previous case the IR camera was shielded by a 9 cm thick polyethylene shield and a 15 mm thick lead shield, along with a 20 mm thick soft iron shield.

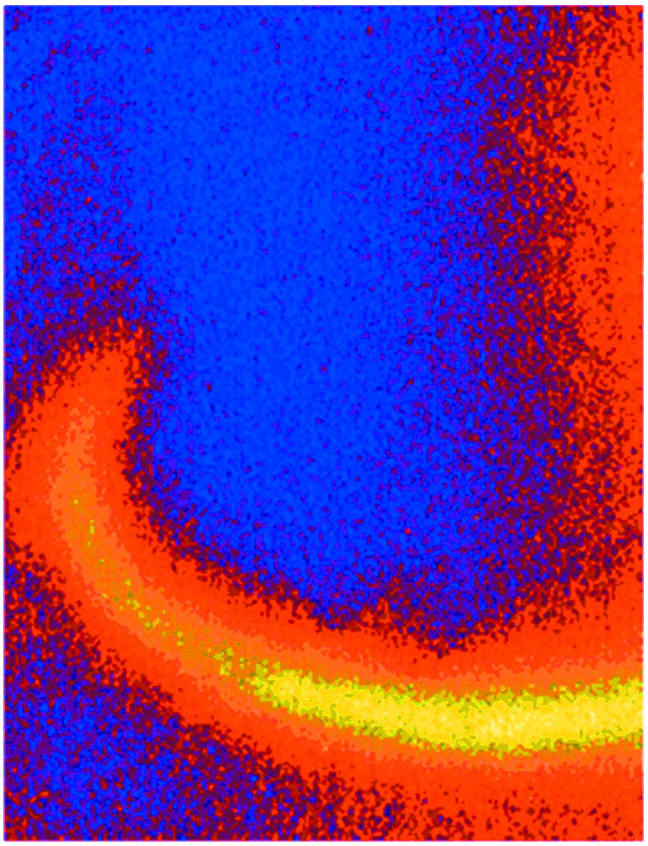

FIG. 2. (Color online) Raw image from Phoenix IR camera showing signal from radiating divertor in JT-60U during shot No. 47832. The number of pixels shown is $\sim 194 \times 258$. A reference image from the beginning of the discharge has been subtracted to remove the signal from background reflections by the foil.

The total neutron fluence from JT-60U D-D operation is estimated to be 10^{16}/s. Modeling predicts that a 10 cm polyethylene shield should reduce the neutron flux by a factor of 10.[19] Compared to the camera location in the previous case, the neutron flux should be a factor of 5 lower. Some problems with the Phoenix IR camera operation have been observed, in particular, communication problems between the IR camera controller and the detector head which is separated form the controller by a 50 ft cable. However it is not clear yet if these problems are due to radiation or some source of noise. We have not noticed any image degradation that could be attributed to gammas or neutrons.

F. IRVB sensitivity

For comparison of the sensitivity of the two IRVBs first we can consider the foil parameters. This can be written in terms of the factor kt_f/κ, which is proportional to the NEPD. By using the calibration factors for kt_f and κ, we get a values of 26.2 J/cm^2 °C for Ta and 9.48 J/cm^2 °C for Au. This means that the Au foil is 2.76 times more sensitive than the Ta foil. If we use Eq. (2) to calculate the NEPD for the two IRVBs we get 700 μW/cm^2 for the previous case with 192 channels and 30 Hz. For the upgrade with the same number of pixels and time response one gets 22.8 μW/cm^2 or a factor of 30 improvement in sensitivity. For a configuration

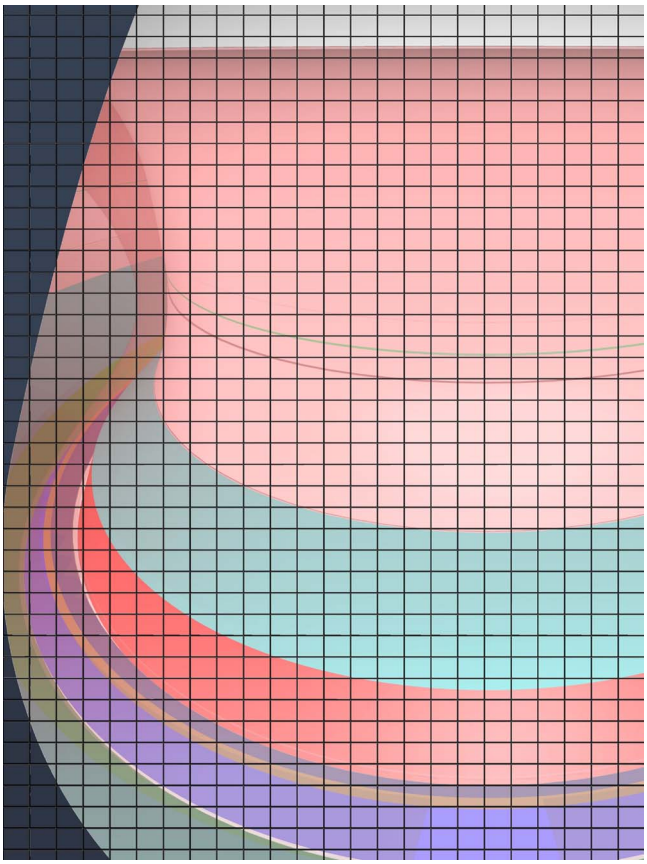

FIG. 3. (Color online) New configuration with the semitangential field of view divided into 40(poloidal)×24(toroidal) pixels. The top of the divertor dome is shown in brown.

with a 10 ms time response and 920 channels this would give a NEPD of 300 $\mu W/cm^2$ or an improvement of 2.3 times over the previous IRVB.

G. Aperture size and spatial resolution

In order to take advantage of the anticipated increase in the sensitivity of the IRVB we reduced the aperture size and in order to increase the number of IRVB channels and improve the spatial resolution. In the previous case the aperture and IRVB pixel size were 5×5 mm^2 and the number of bolometer pixels were 16(vertical/poloidal)×12(horizontal/toroidal). In the new design the aperture size is decreased to 2 mm(vertical)×2.5 mm (horizontal) to give a fivefold increase in the number of IRVB pixels to 40(vertical/poloidal)×24(horizontal/toroidal) or a total of 960 IRVB pixels. The position of the aperture with respect to the foil did not change and therefore the total field of view of the IRVB (shown in Fig. 3), but rather is subdivided into a larger number of smaller pixels as described above. This reduction in the size of the aperture area (and bolometer pixel area) by a factor of 5 reduces the signal level by a factor of 25, but this should be compensated by the increase in the sensitivity of the IRVB as described above. The spatial resolution of the field of view of the line averaged brightness in the divertor region should be improved by a factor of 2.5 in the poloidal direction to 6 cm and by a factor of 2 in the toroidal direction to 7.5 cm. This poloidal spatial resolution will be about two times larger than that of the resistive bolometers.

H. Time resolution

The time resolution of the imaging bolometer is not only ultimately limited by the frame rate of the IR camera but also by the time constant of the diffusion in the foil (thermal diffusivity, κ). Since the frame rate of the Phoenix IR camera is 345 Hz it is possible to investigate much faster phenomena than was the case with the 30 Hz Omega IR camera; however, this higher time resolution comes at the cost of sensitivity as can be seen from Eq. (2) where $S\sim f_{bol}^{3/2}$. Also with the Phoenix IR camera it is possible to reduce the image window size and thereby the number of pixels and readout the reduced image faster since the pixel readout time is limiting the frame rate. As an example, the 40(vertical)×24(toroidal) channel full frame bolometer image can be reduced to a 17×1 channel bolometer array with the same size bolometer pixels (2×2 mm^2), which can be sampled at 5574 frames/s, but the resulting NEPD is an unacceptably high value of 2.7 W/cm^2.

IV. CONCLUSIONS AND DISCUSSION

We have produced an imaging bolometer with 40×24 (920) channels and a time response of 10 ms with a NEPD of 0.3 mW/cm^2. This is 2.3 times better than the NEPD of the previous IRVB with 16×12 channels and a time response of 33 ms. Since the aperture area was reduced by a factor of 5, the signal is reduced by a factor of 25. Therefore it will be difficult to achieve the design values for the IRVB due to a factor of 10 reduction in signal to noise ratio (S/N). Part of the reason for this reduction was an unanticipated increase by a factor of 2 of the kt_f calibration factor for the Ta foil obtained in the calibration compared to the nominal value, leading to a factor of 2 decrease in the sensitivity. It is not clear why this factor increased so much. We had seen variations in this factor from nominal values for Au foils presumably due to the graphite blackening, but such a large difference is extraordinary. To remedy this it is possible to reduce the number of channels or increase the resolution time; however, decreasing the number of channels (thus increasing the bolometer pixel size) without increasing the aperture size correspondingly is not an optimal arrangement in terms of increasing the S/N.

For a comparison of the NEPD with the resistive bolometers, we use as a reference the number quoted for a resistive bolometer by Mast *et al.*[2] of 1 $\mu W/cm^2$ for a 4 μm gold foil on a Kapton substrate with a time response of 10 ms. To convert this to a 4 μm Pt foil on a SiN substrate we use the assertion of Giannone *et al.*[7] that it would be 3.6 times more sensitive than the Au/Kapton version to get 0.28 $\mu W/cm^2$. For a comparable IRVB with 100 channels based on our experimental results from JT-60U and using the currently most advanced IR camera commercially available (FLIR SC8000, InSb, 1024×1024 pixels, 132 frames/s, ~25 mK) we get 29 $\mu W/cm^2$ or a factor of 100 greater than the Pt/SiN resistive bolometer. However, it should be noted that the

result of Mast *et al.* is rarely obtained in experiment where the NEPD is typically a factor of 10 higher.[20] In any case the sensitivity of the IRVB with 100 channels is still a factor of 10 or lower than an equivalent resistive bolometer. In addition there are other benefits to the resistive bolometers that were not pointed out earlier. The compact size and wire cabling permit installation in positions remote from the port plugs which is beneficial for the tomographic inversion. The installation of an IRVB would be limited to the port plugs and would therefore have to rely on a tangential view and the assumption of toroidal symmetry to achieve the tomographic inversion. Even in this case it is not clear if the spatial resolution requirement for ITER of 5 cm in the divertor could be met by one or two IRVBs and if so, how many channels would be necessary. This would need to be addressed by tomographic modeling. While, on the other hand, the current design for the resistive bolometers on ITER should easily meet the ITER measurement requirements.[4] The other advantage of the resistive bolometers is the *in situ* calibration which has been developed and built in to the amplifiers to permit postshot *in situ* calibration.[4] For the IRVB the initial in-laboratory laser calibration of the foil is very time consuming with the development of 900 separate finite element models necessary in order to measure the calibration coefficients at 80 points on the foil. It would be possible to develop an *in situ* calibration similar to what was performed previously on JT-60U (Ref. 12) and automate the calibration data analysis process, but this would take much development work. Another issue facing both types of bolometers is the differentiation of photon signal from the nuclear heating of the foil. For the IRVB it is envisioned that a checkerboard-patterned mask could be used to remove the photon contribution leaving only the nuclear heating, but this would reduce the number of channels by up to a factor of 2. Also this would require that the nuclear heating and the foil's response to it be uniform on the scale length of the mask dimension. For the resistive bolometers the reference channels could be used to subtract off the nuclear heating contribution, but that would require that both reference and sensing foils be matched in terms of their response to nuclear heating and that the nuclear heating be uniform over the dimension separating the reference and sensing foils. This issue is being addressed for the resistive bolometers through neutronics modeling,[4] and could also be addressed for the IRVB in the same way. Therefore, if the issue of vacuum risk can be set aside and the issues of foil thickness and signal drift can be resolved, then resistive bolometers seem to be the clear choice for a bolometer diagnostic for ITER. However if these are not the case then an IRVB should be considered after evaluating tomography and nuclear heating issues.

In addition to further improvements in IR technology, another prospect for increasing the sensitivity of the IRVB and improving the diagnotic is high temperature operation, based on several points. First of all, for the InSB detector the 3–5 mm wavelength range indicates an optimal target temperature of 750–1430 °C from Planck's law. Therefore we expect an increase in the sensitivity of the IR camera with an increase of the foil temperature up to this range. However, so far, when comparing the Phoenix IR camera at 30 and 150 °C we do not see a significant difference in the noise equivalent temperature. A second benefit of high temperature operation is seen from the Stefan–Boltzmann law, which when differentiated with respect to temperature gives a signal-temperature differential which is proportional to T^3. Third, the contribution of the temperature dependent term to the NEPD [not shown in Eq. (2)] does not become significant until the temperature reaches 1000 °C or greater. Therefore we should be able to increase the operating temperature of the IRVB up to the operating temperature of the ITER first wall (~800 °C) and increase the sensitivity without increasing the NEPD. We plan to test this in the near future.

ACKNOWLEDGMENTS

This work was supported in part by a Grant-in-Aid for Science Research from the Japanese Ministry of Education, Culture, Sports, Science and Technology, "Priority Area of Advanced Burning Plasma Diagnostics" (Grant-in-Aid No. 16082207).

[1] A. W. Leonard, W. H. Meyer, B. Greer, D. M. Behne, and D. N. Hill, Rev. Sci. Instrum. **66**, 1201 (1995).
[2] K. F. Mast, J. C. Vallet, C. Andelfinger, P. Betzler, H. Kraus, and G. Schramm, Rev. Sci. Instrum. **62**, 744 (1991).
[3] L. C. Ingesson, B. Alper, B. J. Peterson, and J. C. Valet, Fusion Sci. Technol. **53**, 528 (2007).
[4] H. Meister, Poster N10, this conference.
[5] T. Nishitani, T. Shikama, R. Reichle, E. R. Hodgson, E. Ishitsuka, S. Kasai, and S. Yamamoto, Fusion Eng. Des. **63–64**, 437 (2002).
[6] M. Gonzalez and E. R. Hodgson, Fusion Eng. Des. **74**, 875 (2005).
[7] L. Giannone, D. Queen, F. Hellman, and J. C. Fuchs, Plasma Phys. Controlled Fusion **47**, 2123 (2005).
[8] K. McCormick, A. Huber, C. Ingesson, F. Mast, J. Fink, W. Zeidner, A. Guigon, and S. Sanders, Fusion Eng. Des. **74**, 679 (2005).
[9] G. A. Wurden, B. J. Peterson, and S. Sudo, Rev. Sci. Instrum. **68**, 766 (1997).
[10] B. J. Peterson, Rev. Sci. Instrum. **71**, 3696 (2000).
[11] B. J. Peterson, A. Yu. Kostrioukov, N. Ashikawa, M. Osakabe, and S. Sudo, Rev. Sci. Instrum. **74**, 2040 (2003).
[12] H. Parchamy, B. J. Peterson, S. Konoshima, H. Hayashi, and D. C. Seo, Rev. Sci. Instrum. **77** 10E515 (2006).
[13] B. J. Peterson, S. Konoshima, A. Yu. Kostryukov, D. Seo, Y. Liu, I. V. Miroshnikov, N. Ashikawa, H. Parchamy, H. Kawashima, N. Iwama, M. Kaneko, the LHD Team, and the JT-60U Team, Plasma Fusion Res. **2**, S1018 (2007).
[14] B. J. Peterson, S. Konoshima, A. Yu. Kostryukov, H. Kawashima, D. C. Seo, I. V. Miroshnikov, T. Omori, N. Ashikawa, H. Parchamy, Y. Liu, and the JT-60 Team, Proceedings of the IEEE 22nd Symposium on Fusion Engineering, 2007 (unpublished), portions reprinted, with permission, ©2007 IEEE.
[15] B. J. Peterson, S. Konoshima, H. Parchamy, M. Kaneko, T. Omori, D. C. Seo, N. Ashikawa, A. Sukegawa, and the JT-60U Team, J. Nucl. Mater. **363–365**, 412 (2007).
[16] H. Parchamy, B. J. Peterson, H. Hayashi, S. Konoshima, N. Ashikawa, D. C. Seo, H. Kawashima, the LHD Team, and the JT-60U Team, Proceedings of the IEEE 22nd Symposium on Fusion Engineering, 2007 (unpublished).
[17] Mikron Infrared Inc., www.mikroninfrared.com
[18] Chiyoda Technol Corporation, www.c-technol.co.jp
[19] A. Morioka, A. Sakasai, K. Masaki, Y. Ishida, N. Miya, M. Matsukawa, A. Kaminaga, and A. Oikawa, Fusion Eng. Des. **63–64**, 115 (2002).
[20] B. J. Peterson, A. Yu. Kostrioukov, N. Ashikawa, Y. Liu, Y. Xu, M. Osakabe, K. Y. Watanabe, T. Shimozuma, S. Sudo, and the LHD Experiment Group, Plasma Phys. Controlled Fusion **45**, 1167 (2003).